1995

Electrowinning of Non-Noble Metals with Simultaneous Hydrogen Evolution at Flow-Through Porous Electrodes II. Experimental

Mahmoud M. Saleh
University of South Carolina - Columbia

John W. Weidner
University of South Carolina - Columbia, weidner@engr.sc.edu

Bahgat E. EI-Anadouli
Cairo University

Badr G. Ateya
Cairo University

Publication Info

Journal of the Electrochemical Society, 1995, pages 4122-4128.

Publisher's link: http://dx.doi.org/10.1149/1.2048474
DOI: 10.1149/1.2048474

Electrowinning of Non-Noble Metals with Simultaneous Hydrogen Evolution at Flow-Through Porous Electrodes

II. Experimental

Mahmoud M. Saleh[a] and John W. Weidner*

Department of Chemical Engineering, University of South Carolina, Columbia, South Carolina, 29208, USA

Bahgat E. El-Anadouli and Badr G. Ateya*

Department of Chemistry, Faculty of Science, Cairo University, Cairo, Egypt

ABSTRACT

This paper presents an interpretation of the experimental results obtained on the electrowinning of zinc at a flow-through porous electrode in light of a mathematical model which was presented in Part I. The process is accompanied by simultaneous hydrogen evolution within the electrode, which increases the pore electrolyte resistivity and decreases the coulombic efficiency. We measured polarization curves, coulombic efficiencies, and current distributions under various conditions of zincate concentrations, flow rates, cell current, and electrode thickness. Reasonable agreement between the measured and predicted current distributions was obtained only under conditions of high electrolyte flow rates, low cell currents, and thinner electrodes. The deviations observed at low electrolyte flow rates and high cell currents are attributed to the agitating effects of the hydrogen gas bubbles, which enhance the local mass-transfer coefficient. This effect was not incorporated in the model due to the absence of adequate correlations.

Introduction

Flow-through porous electrodes have been used in the removal of heavy metal ions from their dilute streams,[1-7] particularly the noble metals (*e.g.*, Cu or Ag) where no gas bubbles are generated within the electrode. Their application to the electrowinning of non-noble metals (*e.g.*, Zn or Cr) faces complications caused by the hydrogen evolution reaction which occurs simultaneously. In addition to lowering the coulombic efficiency of the process, the generation of hydrogen gas bubbles affects the current distribution within the porous electrode and its polarization behavior.[8,9] The effects of gas bubbles on the polarization, current distribution, and mechanism of mass transfer are well documented on planar electrodes.[10-14] They have not been quantified in porous electrodes.

The electrowinning of non-noble metals coupled with hydrogen evolution is an especially important case of simultaneous reactions in porous electrodes. Alkire *et al.*[15,16] developed a mathematical model for predicting the current and potential distributions within porous electrodes in the presence of simultaneous homogeneous and heterogeneous reactions. They studied three types of reactions, simultaneous deposition of metals from a mixture of their ions, deposition of metals in the presence of a redox reaction, and an electro-organic synthesis. However, in this treatment, no gas evolution was considered. More recently Ateya *et al.*[17] experimentally evaluated the parameters affecting the electrowinning of zinc from alkaline zincate solutions with simultaneous hydrogen evolution at flow-through porous electrodes, but offered no theoretical interpretation of the experimental results. Several other work-

* Electrochemical Society Active Member.
[a] Present address: Department of Chemistry, Cairo University, Cairo, Egypt.

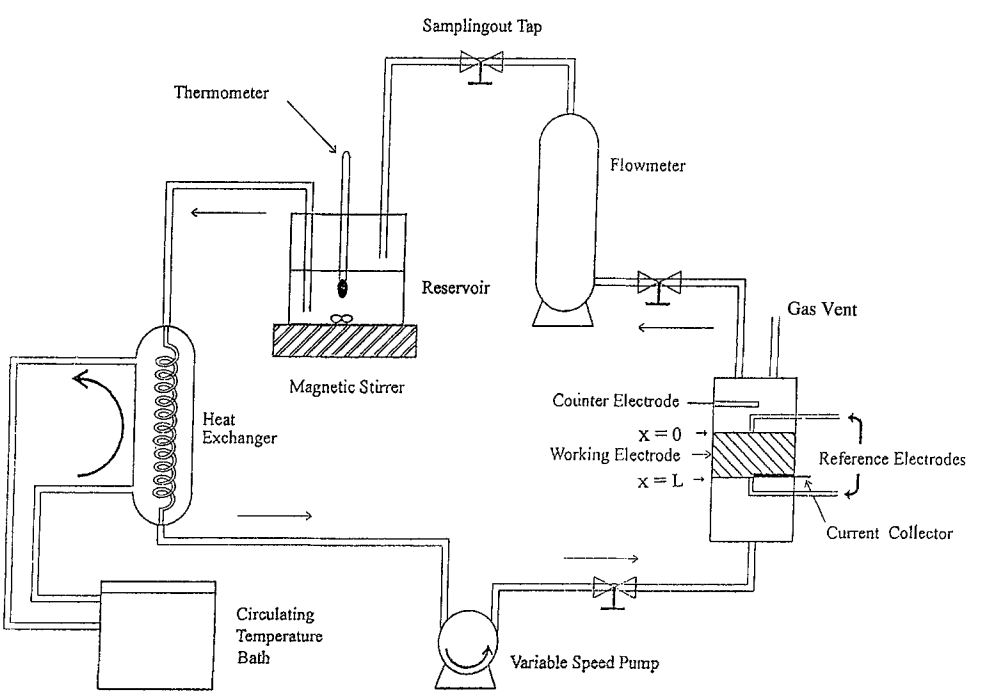

Fig. 1. Schematic of the flow system and electrolytic cell.

ers have also treated the deposition of zinc from alkaline zincate solutions at porous electrodes.[18-21]

The objective of the present paper is to offer a quantitative interpretation of the effects of some parameters and operating conditions on the polarization behavior and current distribution within a flow-through porous electrode operating on the electrowinning of zinc from an alkaline zincate solution. The experimental results are compared to the predicitons of a mathematical model[22] which takes into consideration: (*i*) the charge-transfer kinetics of both the zinc deposition and the hydrogen evolution reactions at the metal/electrolyte interface, (*ii*) the mass-transfer limitations of the zinc deposition reaction, and (*iii*) the effects of the evolving hydrogen gas bubbles on the resistivity of the pore electrolyte.

Experimental

Figure 1 is a scheme of the flow system and cell arrangement. The system consists of a reservoir made of polypropylene plastic which contains a thermometer and a heat exchanger to control the temperature and a magnetic stirrer to mix the solution during circulation. The solution was circulated using a variable speed pump and the flow rate was measured using a floating sphere-type flowmeter. Samples were collected at time intervals of 10 min and analyzed for the concentration of zincate using an atomic adsorption spectrophotometer. The working electrode was made of galvanized stainless steel screens (*i.e.*, Zn/stainless steel with 0.05 cm diameter wire. The number of screens was 10, 20, or 28 with an average bed thickness, L, of 0.8, 1.6, or 2.1 cm, respectively. The packed bed electrode had a specific surface area of 20.0 cm^{-1}, a porosity of 0.80, a diameter of 1.6 cm, and an ohmic resistance < 0.01 Ω. The counterelectrode was made of a platinum screen and was placed on the downstream side of the porous electrode. Both reference electrodes were Hg/HgO/1 *M* KOH. With the two reference electrodes, it is possible to measure the potential at the entry and the exit faces of the electrode. The potential reported here is that of the electrode relative to the down-stream reference electrode (denoted as E). Current densities are reported on the basis of the geometrical cross-sectional area of the electrode (*i.e.*, 2.0 cm^2). A potentiostat (EG&G Princeton Applied Research Model 273A) was used in all measurements. A current interrupter technique was used to compensate for the IR drop between the reference electrode and the exit face of the working electrode. The distribution of the zinc reaction current was determined by measuring the weight gain of each screen after a period of 20 min. The screens were removed carefully to avoid mechanical loss of the deposited zinc. The zincate solutions were prepared by dissolving the desired weights of ZnO in KOH of the appropriate concentration. They were deaerated by bubbling pure nitrogen gas. The measurements were performed at 25°C.

Results and Discussion

Model equations.—The simultaneous reactions involved in the electrowinning of zinc from an alkaline zincate are

$$Zn(OH)_4^{-2} + 2e^- = Zn + 4\ OH^- \quad E^\circ = -1.29\ V\ (SHE) \qquad [1]$$

$$2H_2O + 2e^- = H_2 + 2\ OH^- \quad E^\circ = -0.83\ V\ (SHE) \qquad [2]$$

The model development, boundary conditions, and solution technique were presented in part I.[22] Hence, only the governing equations are presented here. The gradient of the zinc solution current is related to the reaction current by

$$\frac{di_{Zn}(x)}{dx} = -j_{Zn}(x) = \frac{-Si_{o,Zn}\,[1 - \exp(2\eta_{Zn}(x)/b)]}{\exp\,[\beta\eta_{Zn}(x)/b] + \dfrac{i_{o,Zn}}{i_{L,Zn}}} \qquad [3]$$

The charge-transfer kinetics involved in Eq. 3 corresponds to a two-electron transfer rate-determining step.[23] The local limiting current density of the zinc deposition reaction, $i_{L,Zn}$, is related to the local mass-transfer coefficient and the bulk concentration by

$$i_{L,Zn} = nFk_mC_{Zn} \qquad [4]$$

The expression for the local mass-transfer coefficient, k_m, was obtained from empirical correlations[24]

$$k_m = 1.17Q^{0.58}\left(\frac{d}{\nu}\right)^{-0.42}\left(\frac{\nu}{D}\right)^{-0.67} \qquad [5]$$

The gradient of the hydrogen solution current is related to the reaction current by

$$\frac{di_H(x)}{dx} = -j_H(x) = -Si_{o,H}\exp[-\alpha\eta_H(x)/b] \qquad [6]$$

where

$$\eta_H(x) = \eta_{Zn}(x) + \Delta E \qquad [7]$$

and $\Delta E = E^\circ_{Zn} - E^\circ_H$. Equation 6 is based on the assumption that Tafel kinetics control the hydrogen evolution reaction. Along with Eq. 3 and 6, Eq. 8 through 11 govern the behavior of the system

$$i(x) = i_{Zn}(x) + i_H(x) \qquad [8]$$

$$i(x) = \kappa(x)\frac{d\eta_{Zn}(x)}{dx} \qquad [9]$$

$$\kappa(x) = \kappa^\circ[\theta - \epsilon(x)]^{3/2} \qquad [10]$$

where, κ°, is the bulk electrolyte conductivity. The gas void fraction is related to the hydrogen solution current by[9]

$$\epsilon(x) = \frac{\theta i_H(x)}{\left(\dfrac{Q}{\sigma}\right) + i_H(x)} \qquad [11]$$

where for ideal gas behavior, σ is given by

$$\sigma = \frac{RT}{2PF} \qquad [12]$$

Table I lists the values of the physical parameters which were used in computing the model predictions. The equilibrium potentials of both the zinc[29] and the hydrogen reactions are given by

$$E^\circ_{Zn} = A_o + A_1 \log M\,[KOH] + A_2 \log M\,[K_2Zn(OH)_4] \qquad [13]$$

$$E^\circ_H = \frac{-2.3\ RT}{F}\,pH \qquad [14]$$

where the As are constants which depend on the temperature and M[KOH] and $M[K_2Zn(OH)_4]$ are the molarities of the hydroxide and zincate, respectively.[29]

Current distribution.—The current distributions of the zinc reaction were measured under different conditions and compared with those calculated from the model. The reaction current was normalized with respect to the cell current and the electrode thickness, *i.e.*, $j_{Zn}(y) = j_{Zn}(x)/(i_{cell}/L)$.[22]

Figure 2 a-c shows comparisons of the measured and predicted effects of the electrolyte flow rate, Q, on the distribution of the zinc reaction current within a packed bed electrode of 0.8 cm thickness operating at a cell current of 0.15 A cm^{-2} on 0.08 *M* ZnO in 3.0 *M* KOH at 25°C. As Q increases, the distribution becomes less uniform. The increase of electrolyte flow rate increases both the limiting current, i_L (Eq. 4, 5), and the bubble product, Q/σ.

Table I. Values of the physical parameters used in computing the model predictions.

Physical parameter	Value used	Literature value	Ref.
$i_{o,Zn}$	6.3×10^{-2} A cm^{-2}	The same value	23
$i_{o,H}$	5.0×10^{-9} A cm s^{-2} [a]	1.0×10^{-9} A cm^{-2}	25
D	1.6×10^{-6} cm^2 s^{-1}	The same value	26
ν	0.015 g · cm^2 · s^{-1}	The same value	27
κ°	0.04 Ω^{-1} cm^{-1}	The same value	28
α	0.5	The same value	25
β	1.0	The same value	23

[a]This value was obtained by fitting the polarization curve of the hydrogen evolution reaction (the blank 3 *M* KOH curve in Fig. 5) to the model prediction in absence of the zinc reaction.

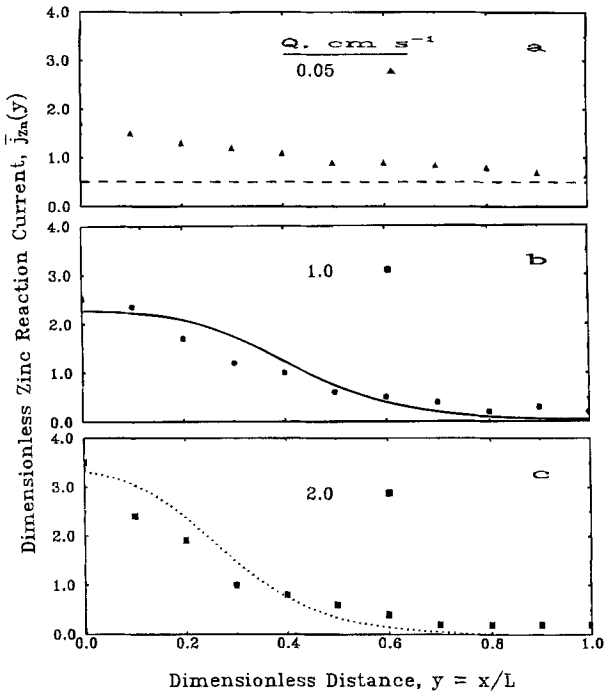

Fig. 2. Zinc reaction current distributions at different electrolyte flow rates. Lines are the model predictions and symbols are the experimental data. L = 0.8 cm; 0.08 *M* ZnO in 3 *M* KOH; i_{cell} = 0.15 A cm^{-2}; T = 25°C.

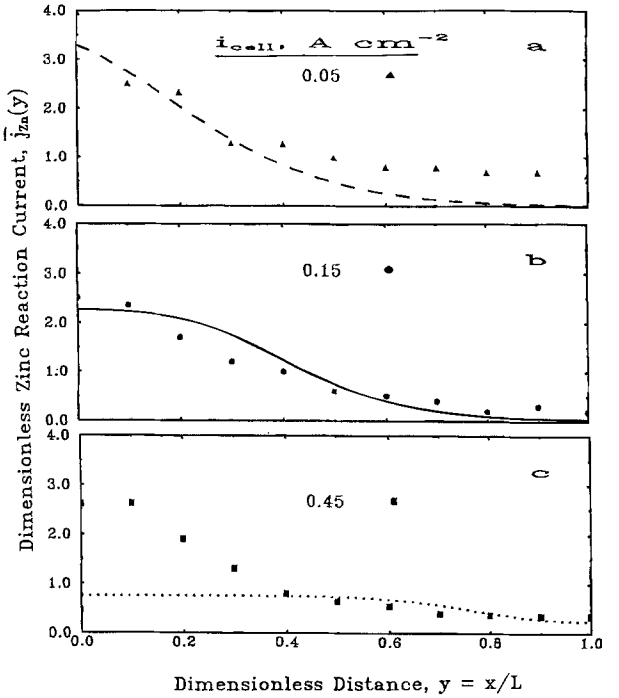

Fig. 3. Zinc reaction current distributions at different cell current densities. Lines are the model predictions and symbols are the experimental data. L = 0.8 cm; 0.08 *M* ZnO in 3 *M* KOH; Q = 1.0 cm s^{-1}; T = 25°C.

It has been shown elsewhere[30] that an increase in i_L leads to a less uniform current distribution, whereas an increase in (Q/σ), leads to a more uniform current distribution. Consequently, the effect of the flow rate, which is observed in Fig. 2 a-c, is the combination of its effects on i_L and Q/σ. Figure 2 a-c shows that the model correctly predicts the shape of the current distributions and gives reasonable agreement with the experimental results at relatively high electrolyte flow rates. At low flow rates, Fig. 2a, the experimentally measured local current densities are is much higher than those predicted particularly toward the exit face of the packed bed electrode. The experimental values approach the predictions further inside the bed. This phenomenon is attributed to the effects of local stirring caused by the generated gas bubbles on the rate of mass transfer and hence on the local limiting current. This effect is much greater near the exit than near the entry face of the electrode. The effect of gas bubbles on the rate of mass transfer is well recognized at planar electrodes.[11,14] Figure 2 a-c shows also that as the flow rate increases, a greater percentage of the cell current is supported by reactions within a smaller fraction of the bed thickness near its exit face.

Figure 3 a-c shows the effects of the cell current on the distributions of zinc reaction current within a packed bed electrode of 0.8 cm thickness for a value of Q = 1.0 cm s^{-1} at 25°C. The model predicts an important effect of the cell current on the distribution of the zinc reaction within the bed. As i_{cell} increases, we observe a limiting current behavior near x = 0 (Fig. 3b, c). The length of this region increases significantly with an increase in the cell current. Over these regions, the model predicts that the zinc reaction is proceeding at its limiting current, *i.e.*, the process is mass-transfer controlled. Since we assumed no concentration gradients in the axial direction, it follows that the theoretically calculated local limiting current is independent of its position within the bed. The value of this local limiting current in A cm^{-2} is the same at x = 0 in both Fig. 3b and c (0.02 A cm^{-2}). On the other hand in Fig. 3a, the predicted currents at x = 0 are less than the above limiting current. Consequently, the predicted nonuniform reaction distribution (dashed line in Fig. 3a) is attributed to ohmic control. The figure shows that reasonable agreement between the model predictions and the experimental data is seen only at i_{cell} = 0.15 A cm^{-2} and to a lesser extent at i_{cell} = 0.05 A cm^{-2}, where we obtained higher discrepancies between the model predictions and the experimental data especially at the back of the electrode. In the case of i_{cell} = 0.45 A cm^{-2}, although the model agrees with the experimental data at the back of the electrode, there is a very large difference between the measured and predicted local currents near and at the exit face of the electrode. This can be attributed to the effects of the evolving hydrogen gas bubbles on the local mass-transfer coefficient. This calls for further studies with appropriate mass-transfer correlations to test the above interpretation and to quantify this effect.

Figure 4a, b shows the effect of the electrode thickness on the zinc reaction current distribution for a flow rate of 1.0 cm s^{-1} and a cell current of 0.15 A cm^{-2}. An increase in the thickness of the electrode leads to a decrease of the dimensionless conductivity group, K (see Table I in the preceding

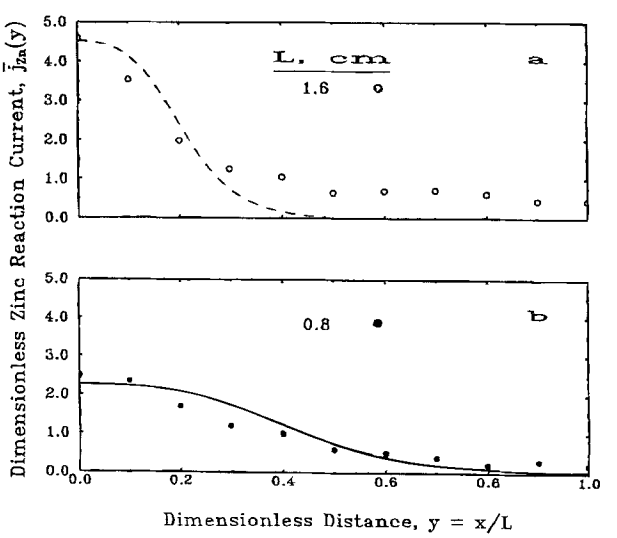

Fig. 4. Zinc reaction current distributions at different electrode thicknesses. Lines are the model predictions and symbols are the experimental data. 0.08 *M* ZnO in 3 *M* KOH; i_{cell} = 0.15 A cm^{-2}, Q = 1.0 cm s^{-1}; T = 25°C.

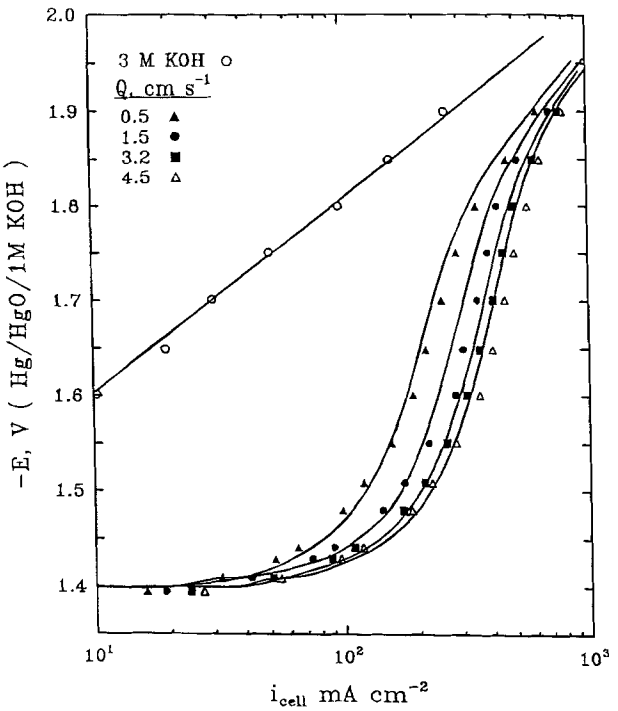

Fig. 5. Current-potential relations at different electrolyte flow rates. Lines are the model predictions and symbols are the experimental data. The potential, E, is the voltage difference between the current collector and the downstream reference electrode. 0.08 *M* ZnO in 3 *M* KOH; T = 25°C.

paper).[22] On the other hand as K decreases, the potential distribution becomes less uniform (see Fig. 4 in the preceding paper).[22] Consequently, as the thickness decreases, the model predicts that the zinc reaction becomes less uniform in agreement with the experimental results obtained in Fig. 4a, b.

From the current distribution results, it is clear that operating at low flow rate has the advantage of uniform reaction and, hence, it leads to a utilization of a larger fraction of the internal surface area of the electrode. However, under this condition mass-transfer restrictions limit the zinc reaction current and lead to a low coulombic efficiency (cf., Fig. 11). The current distribution shows to what extent the internal surface area is used. At nonuniform reaction distribution, using thicker electrode is not preferable because the internal surface area is under utilized.

Polarization curves.—The overall behavior of the electrode can be studied by analyzing the polarization curves for the zincate reaction under different conditions. The current-potential relations were measured at different electrolyte flow rates and zincate concentrations and compared to the theoretical predictions. Table I lists the parameters used in the calculations. The packed bed used in this section was 2.1 cm thick.

Figure 5 shows a comparison between the measured and predicted effects of the electrolyte flow rate on the current-potential relations for the reduction of zincate using 0.08 *M* ZnO in 3 *M* KOH at 25°C. The blank curve was measured to enable us to calculate the partial hydrogen and zinc currents as shown below. The potential of interest here is that at the exit face of the electrode, which is shown in Fig. 5, the current from the blank electrolyte (3 *M* KOH) is due to the hydrogen evolution reaction which results from the reduction of water (see Eq. 1). The current from the zincate solution, i_{cell}, is the sum of the hydrogen evolution current $i_H|_{x=0}$ and of zincate reduction current $i_{Zn}|_{x=0}$ (see Eq. 1, 2). Therefore

$$i_{cell} = i_{Zn}|_{x=0} + i_H|_{x=0} \quad [15]$$

where $i_{Zn}|_{x=0}$ and $i_H|_{x=0}$ are the solution currents at the front of the electrode for the zinc and hydrogen reactions, respectively. In using Eq. 15 to calculate the net current of the zinc reduction reaction, it is assumed that the presence of zincate ions in the electrolyte does not interfere with the kinetics of the hydrogen evolution reaction.[27]

Figure 5 reveals that as the potential increases in the negative direction, the cell current increases. While the polarization curve for the blank electrolyte shows a progressive increase of the cell current with the potential, the zincate curves show rather poorly defined limiting currents and at high enough potentials the hydrogen reaction becomes more significant. As the flow rate increases, at a given potential, E, the cell current increases. Satisfactory agreement between the model predictions and experimental results is generally observed in Fig. 5. It is noteworthy that the experimental results of Fig. 5 correspond to fairly large values of the bubble group, Γ. For instance, at a cell current of 800 mA cm^{-2} and a flow rate of 0.5 cm s^{-1}, Γ = 5. Alternatively, at a cell current of only 100 mA cm^{-2} and a flow rate of 0.5, Γ = 40. These values of Γ correspond to small values of the gas void fraction, ϵ, as deduced from the Fig. 9 in the preceding paper.[22]

Figure 6 shows the effect of the flow rate on the polarization curves of zincate reduction. The currents i_{Zn} in Fig. 6 were determined experimentally from Fig. 5 using Eq. 15. The relations give well-defined limiting currents with values dependent on the electrolyte flow rate.

Figure 7 shows the effect of the zincate concentration on the current-potential relations for zincate reduction at a value of Q = 1.5 cm s^{-1}. As the zincate concentration increases, the cell current increases. Figure 8 shows the relationships between the net zinc current, i_{Zn}, and the potential, E. The value of the limiting current is dependent on the zincate concentration. The agreement between measured and predicted relations is satisfactory.

A summary of the limiting current dependence on the electrolyte flow rate and zincate concentration is shown in Fig. 9 and 10, respectively. The figures contain experimental data (symbols) and model predictions (solid lines) which show satisfactory agreement. The fact that we did not obtain linear relations in either case, points to the complex effects of both variables on the extent of nonuniform distributions of the reaction within the electrode.

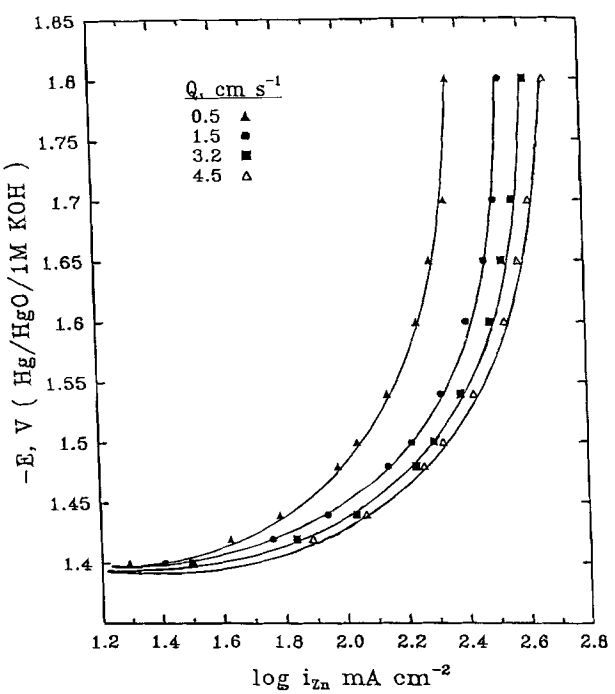

Fig. 6. Zinc current-potential relations at different electrolyte flow rates. Lines are the model predictions and symbols are the experimental data. 0.08 *M* ZnO in 3 *M* KOH; T = 25°C.

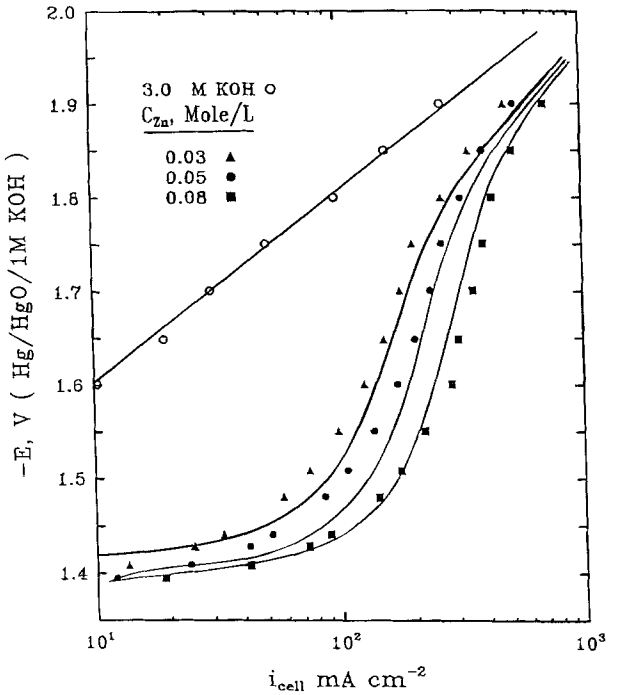

Fig. 7. Current-potential relations at different zincate concentrations. Lines are the model predictions and symbols are the experimental data. The potential, *E*, is the voltage difference between the current collector and the downstream reference electrode. ZnO in 3 *M* KOH; $Q = 1.5$ cm s^{-1}; $T = 25$°C.

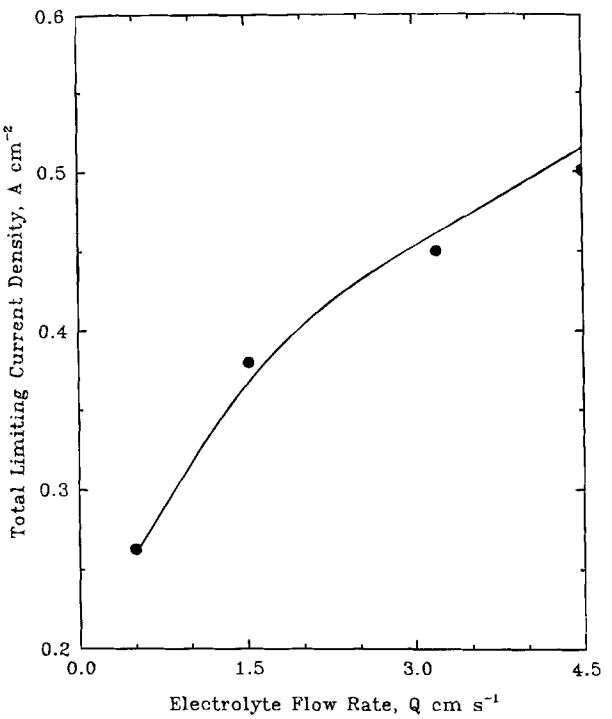

Fig. 9. Effect of electrolyte flow rate on zinc total limiting current. Solid circles are the experimental values and solid lines are the model predictions. 0.08 *M* ZnO in 3 *M* KOH; $T = 25$°C.

Coulombic efficiency.—The total coulombic efficiency of the cathodic current in achieving the electrowinning of zinc is given by

$$\xi_{total} = \frac{i_{Zn}|_{x=0}}{i_{Zn}|_{x=0} + i_{H}|_{x=0}} \quad [16]$$

The data in Fig. 5 and 7 were analyzed to give the efficiency, ξ_{total}, as a function of the cell current at various electrolyte flow rates and zincate concentrations. The results are shown in Fig. 11 and 12, respectively. The coulombic efficiency was calculated using two experimental techniques: (*i*) by separating the partial hydrogen and zinc currents, using Eq. 15 and Fig. 5 and 7 and (*ii*) by measuring the change in the zincate concentration before entering and after exiting the electrode and using Faraday's law. Both techniques gave essentially the same value of coulombic efficiency, within the limits of experimental errors, *e.g.*, 0.80 *vs.* 0.78 for one set of conditions.

Figures 11 and 12 show that both the flow rate and the zincate concentration have strong effects on the coulombic

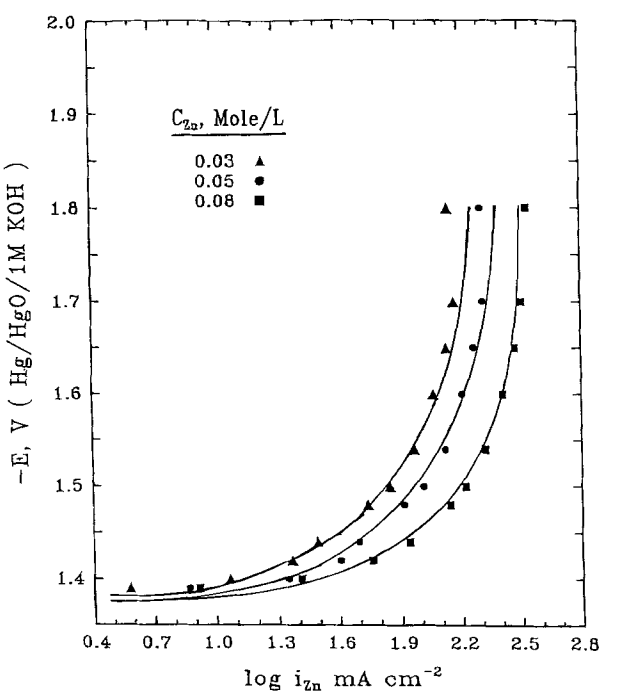

Fig. 8. Zinc current-potential relations at different zincate concentrations. Lines are the model predictions and symbols are the experimental data. ZnO in 3 *M* KOH; $Q = 1.5$ cm s^{-1}; $T = 25$°C.

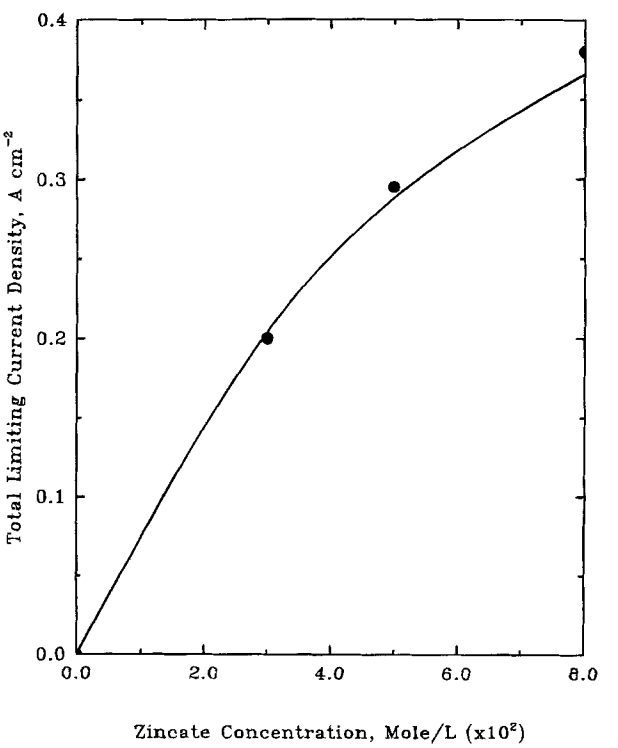

Fig. 10. Effect of zincate concentration on zinc total limiting current. Lines are the model predictions and symbols are the experimental data. ZnO in 3 *M* KOH; $Q = 1.5$ cm s^{-1}; $T = 25$°C.

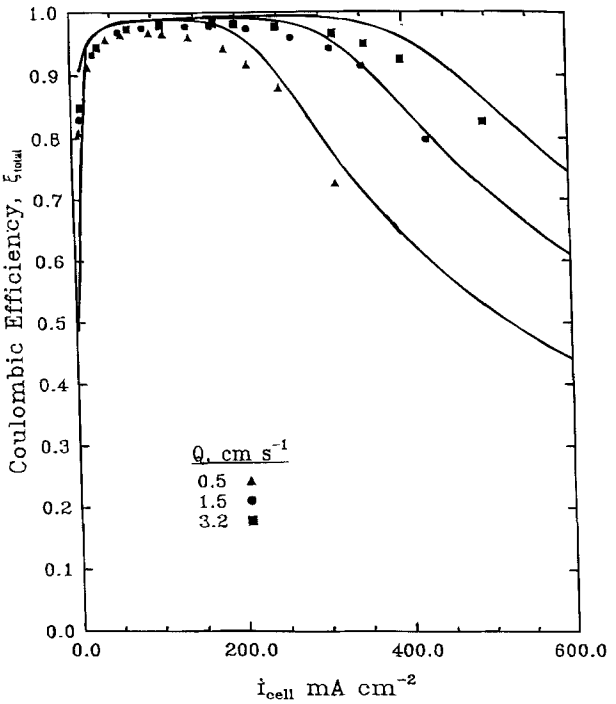

Fig. 11. Effect of electrolyte flow rate on zincate coulombic efficiency. Lines are the model predictions and symbols are the experimental data. 0.08 *M* ZnO in 3 *M* KOH; *T* = 25°C.

efficiency-cell current relations. As the cell current increases the coulombic efficiency increases until it reaches a region of a maximum value and then decreases with further increase in the cell current. The width of this maximum region increases with the increase in flow rate or zincate concentration. The maximum corresponds to the limiting current of the zinc reduction reaction. Before the limiting current is reached, as the cell current increases the polarization increases. Since the sensitivity of the zinc reaction current to the polarization is larger than that of the hydrogen current ($\alpha = \beta/2 = 0.5$, see Table I), the coulombic efficiency increases with the cell current.[22] Because the zinc reaction is mass-transfer limited and its current cannot increase above its limiting value, the increase in cell current beyond this limiting value is supported by the hydrogen evolution reacton and hence the coulombic efficiency decreases.

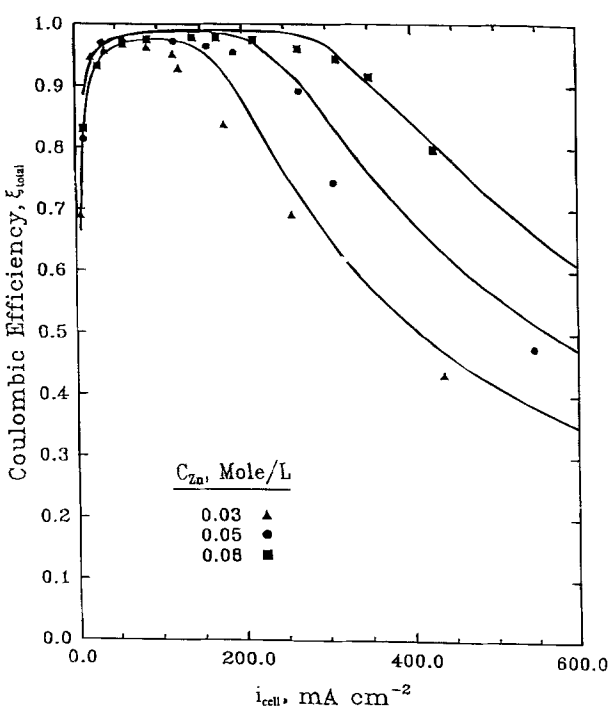

Fig. 12. Effect of zincate concentration on zinc coulombic efficiency. Lines are the model predictions and symbols are the experimental data. ZnO in 3 *M* KOH; *Q* = 1.5 cm s^{-1}, *T* = 25°C.

Figures 11 and 12 reveal two interesting effects of the increase in both the flow rate and the zincate concentration.

1. The maximum value of the total coulombic efficiency, ξ, increases. This is attributed to the fact that the limiting current of the zincate reduction increases with the flow rate and the zincate concentration (see Fig. 9 and 10), whereas the hydrogen current is independent of either variable.

2. Beyond the maximum, the total coulombic efficiency decreases with increasing current more slowly such that there is a broader range of electrowinning currents over which the current efficiency remains high and relatively constant to an extent dependent on the flow rate and zincate concentration. This result is attributed to the higher values of the limiting current (obtainable at higher flow rate or zincate concentration), which make the denominator of Eq. 16 less sensitive to changes in i_H than what is obtainable at small values of the limiting current.

Conclusions

The mathematical model presented in part I of this study gives an interpretation of the experimental results presented here. Reasonable agreement between the model predictions and the experimental results were obtained only when the cell was run at low cell currents (*i.e.*, at or below the limiting current) and at high electrolyte flow rates. At high cell currents or low flow rates, the model predicts lower zinc reaction currents than experimentally measured. This may be attributed to the localized agitating effects of the evolving gas bubbles which enhance the local mass-transfer coefficient. This effect of gas bubbles was not incorporated in the model due to the lack of such correlations, even though their effects on the resistivity of the pore electrolyte were incorporated. This stirring effect of the gas bubbles calls for solution of the model equations with more appropriate mass-transfer correlations.

When the zinc reaction is under mass-transfer control, the coulombic efficiency is enhanced by increasing both the electrolyte flow rate and the zincate concentration. The advantage of operating the cell near the limiting current is that both the cell current and coulombic efficiency are high. This enables one to achieve a high zinc recovery rate at the expense of a continuous decrease in the efficiency of the cell with time as the zincate concentration decreases. This leads to the appearance of time effects which are treated in another article.

Acknowledgment

The authors thank the Egyptian Cultural and Educational Bureau (Washington, DC) for supporting this work through a scholarship to M. Saleh. This work was initiated while B. G. Ateya held a senior Fulbright Fellowship. He gratefully acknowledges the support of the U.S.-Egyptian Binational Fulbright Commission (Cairo, Egypt) and the Council for International Exchange of Scholars (Washington, DC).

Manuscript submitted Feb. 21, 1995; revised manuscript received July 11, 1995.

The University of South Carolina assisted in meeting the publication costs of this article.

LIST OF SYMBOLS

As	constants taken from Ref. 29
b	RT/F, V
d	screen thread diameter, cm
C_{Zn}	zincate ion concentration in the bulk solution, g-mol/cm^3
D	diffusion coefficient of the zincate ion, cm^2 s^{-1}
E	potential, V
$E°$	reversible potential of the electrochemical reaction, V
F	Faraday's constant, 96,500 C eq^{-1}

i_o exchange current per unit reaction area, A cm^{-2}
i_{cell} cell current per unit bed area, A cm^{-2}
$i_{L,Zn}$ zinc local limiting reaction current per unit reaction area, A cm^{-2}
$I_{L,Zn}$ zinc mass-transfer limiting current density, A cm^{-2}
$j_{Zn}(y)$ dimensionless zinc reaction current = $j_{Zn}(x)/(i_{cell}/L)$
k_m local mass-transfer coefficient, cm s^{-1}
L electrode thickness, cm
Q electrolyte velocity, cm s^{-1}
S specific surface area, cm^{-1}
T temperature, K
x distance at a point inside the packed bed, cm
y dimensionless distance at a point inside the packed bed
α charge-transfer coefficient of HER
β charge-transfer coefficient of metal reduction
ξ coulombic efficiency
ϵ the gas void fraction of the pore volume, dimensionless
κ pore electrolyte conductivity, Ω^{-1} cm^{-1}
κ^o conductivity of the bulk electrolyte, Ω^{-1} cm^{-1}
Γ bubble group, $2PFQ/RT$, A cm^{-2}
ν kinematic viscosity, g · cm^2 s^{-1}
θ porosity
η_{Zn} zinc reaction overpotential, V
η_H hydrogen evolution reaction overpotential, V
σ const. = $RT/2PF$ = 0.127 cm^3/C at standard temperature and pressure

REFERENCES

1. J. N. Bennion and J. Newman, *J. Appl. Electrochem.*, **2**, 113 (1972).
2. J. Van Zee and J. Newman, *This Journal*, **124**, 706 (1977).
3. J. Wang and H. D. Dewald, *ibid.*, **130**, 130 (1983).
4. A. T. Kuhn, *J. Appl. Electrochem.*, **4**, 69 (1974).
5. Y. Oren and A. Soffer, *Electrochim. Acta*, **28**, 1649 (1983).
6. R. Alkire and B. Gracon, *This Journal*, **122**, 1594 (1975).
7. J. A. Trainham and J. Newman, **124**, 1528 (1977).
8. B. E. El-Anadouli, and B. G. Ateya, *J. Appl. Electrochem.*, **22**, 277 (1992).
9. B. G. Ateya and B. E. El-Anadouli, *This Journal*, **138**, 1331 (1991).
10. L. J. Janssen and G. J. Visser, *ibid.*, **21**, 753 (1991).
11. H. M. Wang, S. F. Chen, and T. J. O'Keefe, *ibid.*, **19**, 174 (1989).
12. P. J. Sides, in *Modern Aspects of Electrochemistry*, No. 18, R. E. White, J. O'M. Bockris, and B. E. Conway, Editors, Plenum, New York (1986).
13. H. Vogt, in *Comprehensive Treatise of Electrochemistry*, Vol. 6, J. O'M. Bockris, B. E. Conway, E. Yeager, and R. E. White, Editors, Plenum Press, New York (1983).
14. K. J. Cathro, *This Journal*, **139**, 2186 (1992).
15. R. C. Alkire and R. Gould, *ibid.*, **123**, 1842 (1976).
16. R. Gould and R. C. Alkire, *ibid.*, **126**, 2125 (1979).
17. M. E. El-Shakre, M. M. Saleh, B. E. El-Anadouli, and B. G. Ateya, *ibid.*, **141**, 441 (1994).
18. C. Cachet, R. Wiart, and J. Zoppas-Ferreira, *Electrochim. Acta*, **38**, 311 (1993).
19. W. G. Sunu and D. N. Bennion, *This Journal*, **127**, 2008 (1980).
20. W. G. Sunu and D. N. Bennion, *ibid.*, **127**, 2017 (1980).
21. J. W. Evans and G. Savaskan, *J. Appl. Electrochem.*, **21**, 105 (1991).
22. M. M. Saleh, J. W. Weidner, and B. G. Ateya, *This Journal*, **142**, 4113 (1995).
23. J. O'M. Bockris, Z. Nagy, and A. Damjanovic, *ibid.*, **119**, 285 (1972).
24. L. E. Cussler, *Diffusion and Mass Transfer*, p. 230, Cambridge University Press, Cambridge (1984).
25. T. S. Lee, *This Journal*, **118**, 1278 (1971).
26. R. D. Naybour, *Electrochim. Acta*, **13**, 763 (1968).
27. J. St-Pierre and D. L. Piron, *This Journal*, **139**, 105 (1992).
28. D. Dobos, *Electrochemical Data*, pp. 242, 267, Elsevier Scientific Publishing Company, Amsterdam (1975).
29. M. G. Isaacson, F. R. McLarnon, and E. J. Cairns, *This Journal*, **137**, 2361 (1990).
30. M. M. Saleh, Ph.D. Thesis, Cairo University, Cairo Egypt (1995).